

# Quantum reservoir computing on random regular graphs

Moein N. Ivaki,<sup>1</sup> Achilleas Lazarides,<sup>2</sup> and Tapio Ala-Nissila<sup>1,2</sup>

<sup>1</sup>Quantum Technology Finland Center of Excellence, Department of Applied Physics, Aalto University, P.O. Box 11000, FI-00076 Aalto, Finland

<sup>2</sup>Interdisciplinary Centre for Mathematical Modelling and Department of Mathematical Sciences, Loughborough University, Loughborough, Leicestershire LE11 3TU, United Kingdom

Quantum reservoir computing (QRC) is a low-complexity learning paradigm that combines the inherent dynamics of input-driven many-body quantum systems with classical learning techniques for nonlinear temporal data processing. Optimizing the QRC process and computing device is a complex task due to the dependence of many-body quantum systems to various factors. To explore this, we introduce a strongly interacting spin model on random regular graphs as the quantum component and investigate the interplay between static disorder, interactions, and graph connectivity, revealing their critical impact on quantum memory capacity and learnability accuracy. We tackle linear quantum and nonlinear classical tasks, and identify optimal learning and memory regimes through studying information localization, dynamical quantum correlations, and the many-body structure of the disordered Hamiltonian. In particular, we uncover the role of previously overlooked network connectivity and demonstrate how the presence of quantum correlations can significantly enhance the learning performance. Our findings thus provide guidelines for the optimal design of disordered analog quantum learning platforms.

*Introduction.* Quantum machine learning leverages principles of quantum computing to enhance and accelerate traditional machine learning algorithms, offering potential breakthroughs in data processing and complex problem solving beyond classical capabilities [1, 2]. The high-dimensional complex space of quantum states and the rich dynamics of quantum channels offer possibilities for designing low-complexity and high-performing platforms for quantum information processing [3, 4]. Quantum reservoir computing (QRC) has recently emerged as a promising approach toward temporal data processing without the need for often inefficient and inaccurate gradient optimization [5–21]. QRC leverages the inherent dynamics of disordered and dissipative quantum systems to learn, predict, and classify various linear and nonlinear temporal tasks, both quantum and classical, including those inspired by human brain functions [22–24]. Essentially, QRC generalizes the classical reservoir learning frameworks such as chaotic liquid state machines and echo-state networks, which are known to significantly reduce the optimization complexity of conventional recurrent neural networks [25–28]. In QRC, a discrete or continuous stream of inputs interacts with a quantum system (the “reservoir”) and the system is then allowed to undergo quantum dynamical evolution described by a completely positive and trace-preserving quantum map [29]. After some time, determined by physical parameters, a set of measurements in the reservoir are post-processed using classical learning techniques. This is then the computing device. One should compare this approach with variational quantum algorithms on noisy systems [30], which can suffer from notorious barren plateaus. In these cases, the optimization complexity diverges rapidly as the number of optimization parameters grows, causing learning to eventually fail and limiting scalability [31–34]. On

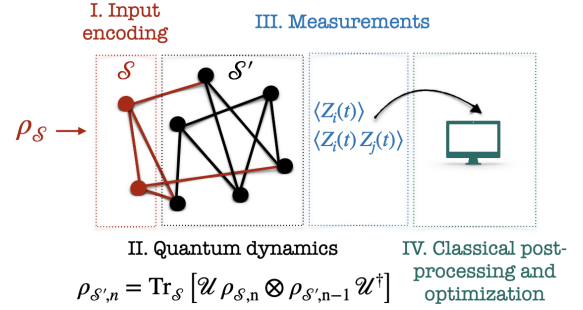


FIG. 1. An auxiliary system  $\mathcal{S}$  is initialized in density matrix  $\rho_{\mathcal{S},n}$ , encoding input data stream at step  $n$ .  $\mathcal{S}$  interacts with the reservoir  $\mathcal{S}'$  for the time-scale  $J^z \Delta t$  through  $\mathcal{U}(\Delta t) = e^{-i\mathcal{H}\Delta t}$ , before the next input is injected. The time-independent Hamiltonian  $\mathcal{H}$  is defined on a graph with  $N$  spins each connected to exactly  $k$  random neighbours. Measurement results of the reservoir degrees of freedom  $\langle \cdot \rangle$ , which are expectation values of spin operators with respect to the current state of the reservoir  $\rho_{\mathcal{S}',n}$ , are then recorded for classical post-processing and optimization purposes. Repeating this for a sequence of temporal data, one can construct a scalable quantum recurrent neural channel  $\rho_{\mathcal{S}',n} = \mathcal{L}_{\mathcal{S}}(\rho_{\mathcal{S}',n-1})$ , capable of learning and emulating various real-world and neurological tasks.

the contrary, QRC systems can *benefit* from noise and dissipation and are much easier to scale up [35–38].

Utilizing disordered, interacting quantum many-body systems as computing reservoirs [5] requires identifying the system setups and parameters which optimize the learning process. To this end, here we study the dependence of learnability performance on the underlying model, in particular, on the connectivity of the spin model and the strength of the interactions and disorder. While previous theoretical studies have focused either on one-dimensional or on fully connected models for

the quantum reservoir, we study spin models defined on random regular graphs (RRGs), and find that the graph degree together with quantum correlations can significantly impact learnability. Notably, in the fully connected limit we observe that some advantages diminish. This is because in this limit the reservoir becomes “too effective” at spreading the information contained in the inputs non-locally while the measurements that are used to feed the classical post-processing are local. Interestingly, it has been shown that for certain spin models, in this densely-connected limit the level statistics demonstrate a suppression of quantum chaos [39], which might be relevant to our findings.

*Model and dynamics.* We consider the following Hamiltonian of interacting quantum spins on a RRG:

$$\mathcal{H} = \sum_{ij,\alpha} J_{ij}^{\alpha} \sigma_i^{\alpha} \sigma_j^{\alpha} + \sum_{i,\alpha} h_i^{\alpha} \sigma_i^{\alpha}, \quad (1)$$

where  $\sigma_i^{\alpha}$  is the Pauli spin-1/2 operator at the vertex  $i$  and  $\alpha \in \{x, z\}$  determines the spin direction. The coupling  $J_{ij}^{\alpha} = J^{\alpha} A_{ij}$ , where  $A_{ij}$  are the matrix elements of the adjacency matrix of the graph. The degree  $k$  of a vertex (site) is defined as the number of edges connected to that vertex, and a RRG is a graph where all vertices have the same degree while the edges are otherwise randomly assigned. Such model Hamiltonian can represent different types of systems, including ion traps, as well as nuclear and electronic spins [40]. We set  $h_i^{\alpha} = h^{\alpha} + \delta_i^{\alpha}$  with  $\delta_i^{\alpha} \in [-\Delta^{\alpha}, \Delta^{\alpha}]$  and fix  $J^z = 1$ ,  $h^z = 0$ ,  $h^x = 1$ ,  $\Delta^z = 0.2$ . The last term ensures the absence of extra Hamiltonian symmetries. All energy and time-scales are given in terms of  $J^z$  and the model is generally non-integrable (including the case  $\Delta^x = J^x = 0$  for  $k > 2$ ).

We separate the total system into the auxiliary system  $\mathcal{S}$  used for data input and the reservoir  $\mathcal{S}'$  (see Fig. 1). Computation is carried out in steps, as follows: Input data is encoded into the density matrix  $\rho_{\mathcal{S}}$  for  $\mathcal{S}$ , and the entire system is set to  $\rho_{\mathcal{S}\mathcal{S}'} \rightarrow \rho_{\mathcal{S}} \otimes \rho_{\mathcal{S}'}$ , where  $\rho_{\mathcal{S}'} = \text{Tr}_{\mathcal{S}}[\rho_{\mathcal{S}\mathcal{S}'}]$ ; thus the ancillary qubits are set to the inputs, and the reservoir is left in a reduced state. The entire system is then allowed to evolve unitarily for the time-scale  $J^z \Delta t$ , and the process is then repeated. Thus after  $n$  input steps, the state of  $\rho_{\mathcal{S}\mathcal{S}'}$  is

$$\rho_{\mathcal{S}\mathcal{S}'}(n\Delta t) = \mathcal{U}(\Delta t) \rho_{\mathcal{S},n} \otimes \rho_{\mathcal{S}'}[(n-1)\Delta t] \mathcal{U}^{\dagger}(\Delta t), \quad (2)$$

with  $\mathcal{U}(\Delta t) = e^{-i\mathcal{H}\Delta t}$ ,  $\rho_{\mathcal{S},n}$  encodes the  $n$ -th input and  $\rho_{\mathcal{S}'}[(n-1)\Delta t]$  is the reservoir state after evolving for  $\Delta t$  after the  $n-1$ -th input step. The quantum map describing this dynamics is strictly contractive, ensuring fading-memory and convergence in an optimal dynamical regime [41]. This resembles the Stinespring representation of a quantum channel, where the evolution of a physical open quantum system can be described as partial trace of a unitary operation on a composite system in a dilated Hilbert space [29]. Alternatively, as a result of

consecutive input injections and resetting, this is equivalent to an incoherent process on the auxiliary system, which can be approximated by local dissipators of rank  $\dim(\mathcal{S})$  [36, 37].

*Training, Learning and Readout.* The input-output relation of a quantum reservoir supplemented with a classical learning layer can be summarized in a functional form as  $\{\bar{y}_n\} = \mathcal{F}(\{\rho_{\mathcal{S},n}\}, \rho_{\mathcal{S}\mathcal{S}',n}, \mathcal{W})$ . Here,  $\{\bar{y}_n\}$  indicates the set of predictions obtained after classical post-processing. These predictions are derived by minimizing an error measure with respect to a sequence of desired targets  $y_n$  through a learning process. During training, the measurements of local expectation values  $\langle \sigma_i^{\alpha}(n\Delta t) \rangle = \text{Tr}[\rho_{\mathcal{S}\mathcal{S}'}(n\Delta t) \sigma_i^{\alpha}]$ , and two-point correlation functions,  $\langle \sigma_i^{\alpha}(n\Delta t) \sigma_j^{\alpha}(n\Delta t) \rangle$ , where  $i, j \in \mathcal{S}'$ , are used as “features”. These features are combined linearly to fit the desired targets  $y_n$ , and the optimal weights  $\mathcal{W}$  are determined by this fitting process. Importantly, we only consider measurements in the computational basis  $\alpha = z$  and *do not* apply time-multiplexing techniques [5], which increases the complexity in number of measurements drastically. Moreover, we do not address the back-action of projective measurements [12, 13, 42]. However, by the virtue of the fading-memory and echo-state properties of a suitable reservoir, a full temporal re-initialization of the system is unnecessary; only the recent state of the system is relevant for making accurate predictions [42, 43]. To quantify the information retrieval accuracy, we employ the Pearson correlation coefficient  $\mathcal{C}_n = \text{cov}^2(y_n, \bar{y}_n) / (\text{var}(y_n), \text{var}(\bar{y}_n))$  [41, 44], where  $\bar{y}_n$  denotes the predicted value at step  $n$ . The coefficient  $\mathcal{C}_n$  is bounded between 1 and 0, indicating complete or no linear correlation between the predicted and target values, respectively. We also estimate prediction accuracy using the averaged mean-squared error, defined as  $\text{MSE} = \sum_n^{N_L} (y_n - \bar{y}_n)^2 / N_L$ , where  $N_L$  is the length of the input data.

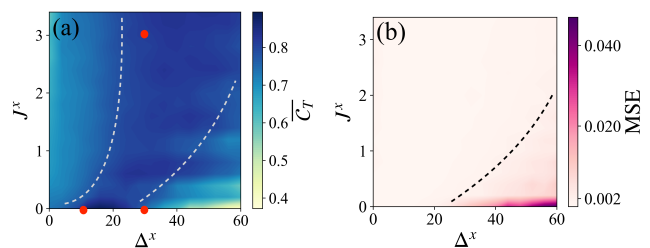


FIG. 2. Learning diagrams. (a) Normalized total memory capacity for  $1 \leq \tau \leq 6$  and (b) MSE for  $\tau = 1$ . Dashed lines approximately mark regions where  $\overline{C}_T \geq 0.75$  and  $\text{MSE} \leq 2.5 \times 10^{-3}$ . Red dots indicate the places in the diagram where most of the analysis in this work is conducted. Evidently, performance is best at the “edge of chaos”, when the system is at the cusp of becoming localized. Calculated for  $(N, k) = (8, 3)$  and  $J^z \Delta t = 3$ .

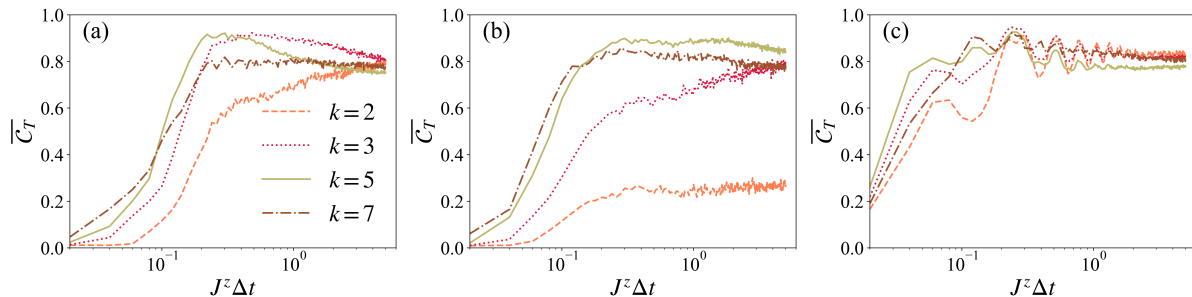


FIG. 3. Behavior of the normalized quantum memory capacity as a function of the interaction time-scale  $J^z \Delta t$ . **(a)**  $(\Delta^x, J^x) = (10, 0)$ , **(b)**  $(\Delta^x, J^x) = (30, 0)$ . **(c)**  $(\Delta^x, J^x) = (30, 3)$ . Calculated for  $N = 8$  and  $1 \leq \tau \leq 6$ . Ordering interactions are particularly crucial for rapidly reaching the asymptotic memory limit and optimizing the functionality of low-degree disordered systems.

Given this discussion, it is clear that the dynamical properties of the reservoir play a pivotal role in learning. In particular, localization behavior of quantum Hamiltonian models defined on RRGs is directly affected by the connectivity, i.e., the graph degree  $k$  [45–47]. Connectivity can also influence the integrability and chaotic properties in certain models [39]. In earlier work it was found that, akin to some classical computation models and for tasks which require both sufficient memory and degree of nonlinearity, QRC systems achieve optimal performance at the *edge of chaos*, or more generally at the vicinity of a (quantum) phase transition [41, 44, 48–51]. Here we will study whether this is also the case in our model.

*Quantum Tomography and Memory.* As our first example, we study a linear quantum task. Consider the following family of bipartite input quantum states, known as Werner states [52, 53]

$$\rho_W(\eta, d, t) = \frac{d-1+\eta(t)}{d-1} \frac{\mathbb{I}}{d^2} - \frac{\eta(t)}{1-d} \mathcal{V}, \quad (3)$$

given as a mixture of a swap operator  $\mathcal{V}$  and a maximally mixed state  $\mathbb{I}$ , with the mixing parameter  $\eta$ . The swap operator is defined as  $\mathcal{V}(|\Psi\rangle \otimes |\Phi\rangle) = |\Phi\rangle \otimes |\Psi\rangle$ , exchanging the states of a bipartite quantum state.  $d$  is dimension of the input and here indicates the number of ancillary qubits. We consider two-qubit input states and can write  $\rho_W(\eta', t) = \frac{1}{4}(1 - \eta'(t))\mathbb{I} - \eta'(t)\rho_B$ , with  $\rho_B = |\Phi\rangle\langle\Phi|$  and  $|\Phi\rangle = (|\uparrow\downarrow\rangle - |\downarrow\uparrow\rangle)/\sqrt{2}$  a singlet Bell state [54, 55]. With  $0 \leq \eta' \leq 1$ ,  $\rho_W$  is entangled for  $\eta' > 1/(d+1)$  and separable otherwise [56, 57]. For a given unitary  $\mathcal{U}$ , this family of bipartite quantum states (by definition) satisfy  $\rho_W = \mathcal{U} \otimes \mathcal{U} \rho_W \mathcal{U}^\dagger \otimes \mathcal{U}^\dagger$ ; a property which is of practical interest in quantum steering and communication protocols [58]. A large family of quantum states, including both Werner and isotropic states, can be expressed in a similar manner, where only a single mixing parameter can characterize the state uniquely. A high fidelity temporal learning of the mixing parameter  $\eta(t)$  is thus a proxy to learning dynamical evolution of

quantum correlations of input states. Generalization of the described learning scheme to higher-dimensional inputs is straightforward and only requires the ability to encode such states. To evaluate the linear memory capacity, we set the learning target to recovering previous inputs,  $y_{n,\tau} \equiv y(n\Delta t - \tau\Delta t) = \eta'(n\Delta t - \tau\Delta t)$ . The total memory capacity for delayed construction of previous inputs is defined as  $\mathcal{C}_T = \sum_{n,\tau} \mathcal{C}_{n,\tau}$ , with  $\tau \geq 0$  an integer specifying the *delay time* and  $\mathcal{C}_{n,\tau}$  the Pearson correlation coefficient for  $y_{n,\tau}$ . We note that the total memory is also bounded and we have  $\mathcal{C}_{n,\tau} \rightarrow 0$  when  $\tau \rightarrow \infty$ . For a fixed finite delay time, we can normalize the averaged total memory and write  $\bar{\mathcal{C}}_T = \mathcal{C}_T/\tau_{\max}$ .

*Optimal Learning Regimes.* Figure 2 displays a learning diagram for  $\bar{\mathcal{C}}_T$  and MSE of the predicted values in the  $\Delta^x - J^x$  plane. The optimal learning regime for our model occurs at around the boundary of chaotic-localized phase transitions. Notably, for a given interaction timescale  $J^z \Delta t$  and for a graph with a fixed degree  $k$ , the addition of interactions  $\sigma_i^x \sigma_j^x$  in the disordered regimes is advantageous to both memory and also short-term prediction accuracy. As we will numerically establish later, this term represents an entangling and delocalizing interaction. The behavior of memory capacity as a function of the  $\mathcal{S} - \mathcal{S}'$  interaction timescale  $J^z \Delta t$  is shown for selected points in Fig. 3. In certain dynamical regimes, there can be a window where the largest memory performance is achieved, in accordance with previous studies [5, 44]. As disorder increases, only high-degree reservoirs exhibit rapid initial growth of memory, followed by saturation in the long-time limit. Interestingly, in this set, the graphs with  $k = 2, 3$  exhibit anomalously slow behavior, which reflects the slow propagation of information in the reservoir in these regimes. Adding the ordering interactions recovers the fast growth of the quantum memory capacity and allows the system to reach the optimal possible performance for all degrees; we attribute this to their delocalizing effect.

The main features discussed above are also evident in Fig. 4, where we additionally observe that, for the

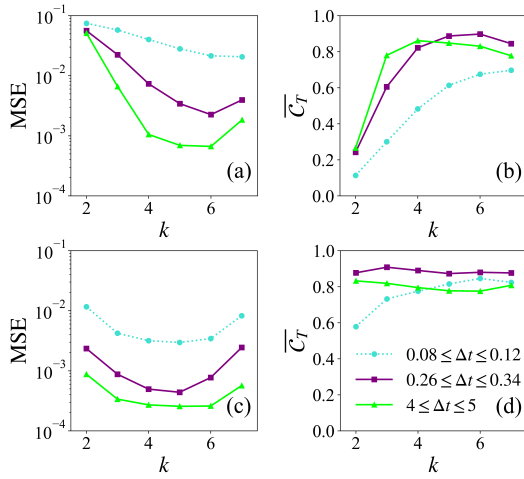


FIG. 4. Time-averaged MSE and normalized total memory capacity as a function of the graph degree  $k$ . **(a)-(b)**  $(\Delta^x, J^x) = (30, 0)$  **(c)-(d)**  $(\Delta^x, J^x) = (30, 3)$ . Memory is reported for  $N = 8, 1 \leq \tau \leq 6$  and MSE for  $\tau = 1$ . Apart from highlighting the role of  $\Delta t$  in our setup, disordered reservoirs achieve the most optimal computing performance, in terms of both accuracy and memory, on intermediate-degree graphs and in presence of quantum interactions.

specified time intervals, higher connectivity elevates the memory capacity and improves the short-term prediction errors. However, the most optimal learning regime, in terms of both memory and accuracy, is achieved by tuning moderate interactions and computing on graphs with an intermediate  $k/N$  ratio. While reservoirs defined on higher degree graphs can evade localization in the presence of stronger disorder, it becomes exceedingly difficult to extract the non-locally hidden inputs information through only (quasi-) local measurements when  $k \rightarrow N - 1$ . In such cases, retrieving the inputs information in a chosen measurement basis possibly requires measuring higher-order correlation functions of the form  $\langle \sigma_i^\alpha \sigma_j^\alpha \cdots \sigma_N^\alpha \rangle$ , which should be useful as extra learnable features in the training stage. Changes in the quantum chaotic behaviour in the highly-connected limit [39] may also be responsible for the drop in learning performance.

*Correlation and Entanglement.* The performance of quantum reservoirs can be related to fundamental and physical measures, such as degree of “quantumness” [9, 59, 60], information scrambling and dynamical correlations [48, 61–63]. Here we study an alternative version of the correlation operator introduced in Refs. [64, 65], and define the auxiliary system-reservoir correlation as  $\chi(t) = \rho_{SS'}(0) - \rho_{SS'}(t)$ , with  $\rho_{SS'}(0) = \rho_S(0) \otimes \rho_{S'}(0)$  and  $\rho_{SS'}(t) = \mathcal{U}(t) \rho_{SS'}(0) \mathcal{U}^\dagger(t)$ . We numerically calculate  $\|\chi(t)\|$ , with  $\|\cdot\|$  the Hilbert-Schmidt norm. This probe measures the degree of total correlation introduced by the dynamics between the initially unentangled  $\mathcal{S}$  and  $\mathcal{S}'$ , and here it can also be interpreted simply as a distance measure. We set  $\rho_S = \rho_W$  with some random  $\eta'$

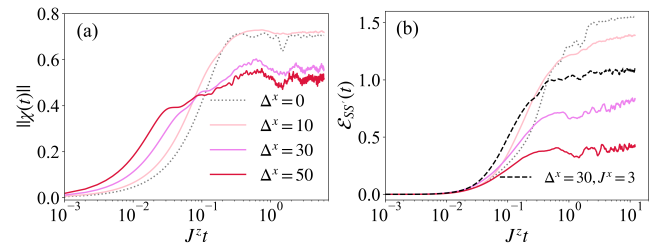


FIG. 5. **(a)** Auxiliary system-reservoir correlation at various disorder strength with  $J^x = 0$ . Controlled disorder can aid in creating complex and richer dynamics. **(b)** Dynamical logarithmic negativity between auxiliary system  $\mathcal{S}'$  and the reservoir  $\mathcal{S}$ . Here  $(N, k) = (8, 3)$ . Entangling quantum correlations are crucial for avoiding localization and improving learning performance.

and average over different realization of initial states and disordered Hamiltonians. As shown in Fig. 5(a), initially  $\|\chi(0)\| = 0$ , indicating no correlation between auxiliary and reservoir degrees of freedom. As time passes by,  $\|\chi(t)\|$  displays an initial growth within the time-scale  $\tau \propto 1/\Delta^x$  for  $\Delta^x/J^z > 1$ . Notably, with an optimal disorder level, composite system can avoid localization while leveraging chaotic dynamics for rapid and enhanced developments of correlations. While being sensitive to certain forms of information localization and the spectral properties of the underlying Hamiltonian, this measure lacks the ability to distinguish between quantum and classical correlations.

A more useful measure of the dynamical quantum correlation build-up is the mixed-state entanglement between the auxiliary system  $\mathcal{S}$  and the reservoir  $\mathcal{S}'$ . We characterize this here by the logarithmic negativity defined as  $\mathcal{E}_{SS'} = \log_2 \|\rho_{SS'}^{T_S}\|$ , where  $T_S$  indicates partial transpose with respect to  $\mathcal{S}$  and  $\|\cdot\|$  is the trace norm [57, 66–69]. Finite logarithmic negativity quantifies entanglement cost and entanglement of distillation [70]. The dynamical behavior of  $\mathcal{E}_{SS'}$  for different disorder strengths is shown in Fig. 5(b). Slow logarithmic growth of entanglement can be attributed to (the onset of) localization, which should support area-law scaling with the system size, as opposed to the usual volume-law scaling in chaotic quantum systems [71]. As can be seen, adding the ordering interactions  $\sigma_i^x \sigma_j^x$  in the large disorder regime recovers the fast growth and produces strong entanglement at short times. The presence of quantum correlations can in turn improve the memory capacity and learnability accuracy of disordered reservoirs, as observed in the previous section.

*Classical Logical Multitasking.* To showcase the ability of our spin reservoir in performing nonlinear tasks, we now consider classical logical multitasking [8]. Given two independent sequences of binary inputs, the network tries to simultaneously learn how to AND, OR and XOR them. We set the state of each input spin to

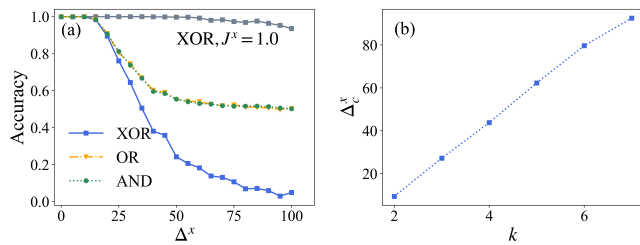


FIG. 6. (a) Accuracy of the logical multitasking as a function of disorder with and without interactions  $\propto J^x$ , shown for  $(N, k) = (8, 3)$  and  $J^z \Delta t = 3$ . Strong disorder degrades the accuracy. (b) Critical disorder strength  $\Delta_c^x$  for the XOR operation as a function of graph degree  $k$ , with the threshold accuracy set to  $\approx 0.7$ , calculated for  $J^x = 0$ . Higher-degree graphs are more resistant to disorder.

$\rho_n = (1 - \eta_n) |\uparrow\rangle\langle\uparrow| + \eta_n |\downarrow\rangle\langle\downarrow|$  with  $\eta_n \in \{0, 1\}$  encoding the input bits. Figure 6 displays the accuracy of the learned operations as the disorder and connectivity are varied. The XOR operation is the only operation that cannot be separated linearly in the two-dimensional input space and shows higher sensitivities to tuning the strength of disorder. However, adding moderate interactions recovers the maximal performance in most regimes, consistent with earlier observations. This supports the expectation that excessive local disorder, in the absence of quantum interactions, can quickly undermine nonlinear information processing capabilities [41]. Remarkably, in this case the critical disorder strength for the accuracy of the XOR to fall just below  $\approx 0.7$  behaves almost linearly as a function of the graph degree, offering a practical tool to control the performance of QRC systems.

*Summary and Discussion.* We have introduced a many-body spin reservoir defined on RRGs and evaluated its learning capabilities for various tasks. Our findings demonstrate that, in an optimal dynamical regime, given in terms of disorder, interactions, and connectivity, our model captures the key properties of a high-performing quantum reservoir without requiring time-multiplexing. Our work paves the way towards designing practical analog QRC platforms by linking their performance to fundamental physical and geometrical properties. In experimental realizations, utilizing spatial-multiplexing for small quantum systems is a practical option [72]. Possibly, a few random measurements can provide enough information to perform a given learning task with high fidelity [73–75]. Additionally, it would be informative to study how different (symmetry) classes of unitary operations [76] and non-trivial electronic topology [77, 78] affect the learning performance. Finally, while here we focused on supervised learning, it is worth exploring the potential for unsupervised approaches for classification tasks.

*Acknowledgements.* We wish to thank Alexander Balanov, Juan Sebastian Toterogongora, Sergey Savielev,

and Alexandre Zagoussin for useful discussions. We acknowledge the support of the UK Research and Innovation (UKRI) Horizon Europe guarantee scheme for the QRC-4-ESP project under grant number 101129663 and the Academy of Finland through its QTF Center of Excellence program (Project No. 312298).

- 
- [1] J. Biamonte, P. Wittek, N. Pancotti, P. Rebentrost, N. Wiebe, and S. Lloyd, *Nature* **549**, 195 (2017).
  - [2] G. Carleo, I. Cirac, K. Cranmer, L. Daudet, M. Schuld, N. Tishby, L. Vogt-Maranto, and L. Zdeborová, *Rev. Mod. Phys.* **91**, 045002 (2019).
  - [3] A. J. Daley, I. Bloch, C. Kokail, S. Flannigan, N. Pearson, M. Troyer, and P. Zoller, *Nature* **607**, 667 (2022).
  - [4] M. Schuld and N. Killoran, *PRX Quantum* **3**, 030101 (2022).
  - [5] K. Fujii and K. Nakajima, *Phys. Rev. Appl.* **8**, 024030 (2017).
  - [6] S. Ghosh, A. Opala, M. Matuszewski, T. Paterek, and T. C. Liew, *npj Quantum Information* **5**, 35 (2019).
  - [7] D. Marković and J. Grollier, *Applied physics letters* **117** (2020).
  - [8] R. A. Bravo, K. Najafi, X. Gao, and S. F. Yelin, *PRX Quantum* **3**, 030325 (2022).
  - [9] A. Senanian, S. Prabhu, V. Kremenetski, S. Roy, Y. Cao, J. Kline, T. Onodera, L. G. Wright, X. Wu, V. Fatemi, *et al.*, arXiv preprint arXiv:2312.16166 (2023).
  - [10] F. Hu, S. A. Khan, N. T. Bronn, G. Angelatos, G. E. Rowlands, G. J. Ribeill, and H. E. Türeci, arXiv preprint arXiv:2312.16165 (2023).
  - [11] P. Mujal, R. Martínez-Peña, J. Nokkala, J. García-Beni, G. L. Giorgi, M. C. Soriano, and R. Zambrini, *Advanced Quantum Technologies* **4**, 2100027 (2021).
  - [12] T. Yasuda, Y. Suzuki, T. Kubota, K. Nakajima, Q. Gao, W. Zhang, S. Shimono, H. I. Nurdin, and N. Yamamoto, arXiv preprint arXiv:2310.06706 (2023).
  - [13] K. Kobayashi, K. Fujii, and N. Yamamoto, arXiv preprint arXiv:2406.15783 (2024).
  - [14] K. Nakajima, *Japanese Journal of Applied Physics* **59**, 060501 (2020).
  - [15] O. Ahmed, F. Tennie, and L. Magri, arXiv preprint arXiv:2405.03390 (2024).
  - [16] K. Fujii and K. Nakajima, *Reservoir Computing: Theory, Physical Implementations, and Applications*, 423 (2021).
  - [17] P. Pfeffer, F. Heyder, and J. Schumacher, *Phys. Rev. Res.* **4**, 033176 (2022).
  - [18] A. Sakurai, M. P. Estarellas, W. J. Munro, and K. Nemoto, *Phys. Rev. Appl.* **17**, 064044 (2022).
  - [19] S. A. Khan, F. Hu, G. Angelatos, and H. E. Türeci, arXiv preprint arXiv:2110.13849 (2021).
  - [20] F. Wudarski, D. O’Connor, S. Geaney, A. A. Asanjan, M. Wilson, E. Strbac, P. A. Lott, and D. Venturelli, arXiv preprint arXiv:2311.14105 (2023).
  - [21] T. Krisnanda, H. Xu, S. Ghosh, and T. C. H. Liew, *Phys. Rev. A* **107**, 042402 (2023).
  - [22] D. Marković, A. Mizrahi, D. Querlioz, and J. Grollier, *Nature Reviews Physics* **2**, 499 (2020).
  - [23] Y. Yamamoto, K. Aihara, T. Leleu, K.-i. Kawarabayashi, S. Kako, M. Fejer, K. Inoue, and H. Takesue, *npj Quantum Information* **3**, 49 (2017).

- [24] F. Tacchino, C. Macchiavello, D. Gerace, and D. Bajoni, *npj Quantum Information* **5**, 26 (2019).
- [25] M. Lukoševičius and H. Jaeger, *Computer science review* **3**, 127 (2009).
- [26] M. Cucchi, S. Abreu, G. Ciccone, D. Brunner, and H. Kleemann, *Neuromorphic Computing and Engineering* **2**, 032002 (2022).
- [27] G. Tanaka, T. Yamane, J. B. Héroux, R. Nakane, N. Kanazawa, S. Takeda, H. Numata, D. Nakano, and A. Hirose, *Neural Networks* **115**, 100 (2019).
- [28] D. J. Gauthier, E. Bollt, A. Griffith, and W. A. Barbosa, *Nature Communications* **12**, 1 (2021).
- [29] F. Caruso, V. Giovannetti, C. Lupo, and S. Mancini, *Rev. Mod. Phys.* **86**, 1203 (2014).
- [30] M. Cerezo, A. Arrasmith, R. Babbush, S. C. Benjamin, S. Endo, K. Fujii, J. R. McClean, K. Mitarai, X. Yuan, L. Cincio, *et al.*, *Nature Reviews Physics* **3**, 625 (2021).
- [31] M. Larocca, S. Thanasilp, S. Wang, K. Sharma, J. Biamonte, P. J. Coles, L. Cincio, J. R. McClean, Z. Holmes, and M. Cerezo, *arXiv preprint arXiv:2405.00781* (2024).
- [32] J. R. McClean, S. Boixo, V. N. Smelyanskiy, R. Babbush, and H. Neven, *Nature Communications* **9**, 4812 (2018).
- [33] C. Ortiz Marrero, M. Kieferová, and N. Wiebe, *PRX Quantum* **2**, 040316 (2021).
- [34] M. Cerezo, M. Larocca, D. García-Martín, N. L. Diaz, P. Braccia, E. Fontana, M. S. Rudolph, P. Bermejo, A. Ijaz, S. Thanasilp, *et al.*, *arXiv preprint arXiv:2312.09121* (2023).
- [35] L. Domingo, G. Carlo, and F. Borondo, *Scientific Reports* **13**, 8790 (2023).
- [36] M. L. Olivera-Atencio, L. Lamata, and J. Casado-Pascual, *Advanced Quantum Technologies* , 2300247 (2023).
- [37] A. Sannia, R. Martínez-Peña, M. C. Soriano, G. L. Giorgi, and R. Zambrini, *Quantum* **8**, 1291 (2024).
- [38] T. Kubota, Y. Suzuki, S. Kobayashi, Q. H. Tran, N. Yamamoto, and K. Nakajima, *arXiv preprint arXiv:2207.07924* (2022).
- [39] A. Grabarits, K. R. Swain, M. S. Heydari, P. Chandarana, F. J. Gómez-Ruiz, and A. del Campo, *arXiv preprint arXiv:2405.14376* (2024).
- [40] I. M. Georgescu, S. Ashhab, and F. Nori, *Rev. Mod. Phys.* **86**, 153 (2014).
- [41] R. Martínez-Peña, G. L. Giorgi, J. Nokkala, M. C. Soriano, and R. Zambrini, *Phys. Rev. Lett.* **127**, 100502 (2021).
- [42] P. Mujal, R. Martínez-Peña, G. L. Giorgi, M. C. Soriano, and R. Zambrini, *npj Quantum Information* **9**, 16 (2023).
- [43] J. Chen and H. I. Nurdin, *Quantum Information Processing* **18**, 1 (2019).
- [44] Q. H. Tran and K. Nakajima, *Phys. Rev. Lett.* **127**, 260401 (2021).
- [45] G. De Tomasi, S. Bera, A. Scardicchio, and I. M. Khaymovich, *Phys. Rev. B* **101**, 100201 (2020).
- [46] K. S. Tikhonov and A. D. Mirlin, *Phys. Rev. B* **99**, 214202 (2019).
- [47] D. Kochergin, I. M. Khaymovich, O. Valba, and A. S. Gorsky, *SciPost Physics* **16**, 106 (2024).
- [48] W. Xia, J. Zou, X. Qiu, and X. Li, *Frontiers of Physics* **17**, 33506 (2022).
- [49] R. Legenstein and W. Maass, *Neural networks* **20**, 323 (2007).
- [50] C. G. Langton, *Physica D: nonlinear phenomena* **42**, 12 (1990).
- [51] J. O’Byrne and K. Jerbi, *Trends in Neurosciences* **45**, 820 (2022).
- [52] R. F. Werner, *Physical Review A* **40**, 4277 (1989).
- [53] R. Uola, A. C. S. Costa, H. C. Nguyen, and O. Gühne, *Rev. Mod. Phys.* **92**, 015001 (2020).
- [54] N. Li, S. Luo, and Y. Sun, *Annals of Physics* **424**, 168371 (2021).
- [55] M. Barbieri, F. De Martini, G. Di Nepi, and P. Mataloni, *Phys. Rev. Lett.* **92**, 177901 (2004).
- [56] M. Horodecki and P. Horodecki, *Phys. Rev. A* **59**, 4206 (1999).
- [57] R. Horodecki, P. Horodecki, M. Horodecki, and K. Horodecki, *Rev. Mod. Phys.* **81**, 865 (2009).
- [58] H. M. Wiseman, S. J. Jones, and A. C. Doherty, *Phys. Rev. Lett.* **98**, 140402 (2007).
- [59] N. Götting, F. Lohof, and C. Gies, *Phys. Rev. A* **108**, 052427 (2023).
- [60] W. D. Kalfus, G. J. Ribeill, G. E. Rowlands, H. K. Krovi, T. A. Ohki, and L. C. G. Govia, *Phys. Rev. Res.* **4**, 033007 (2022).
- [61] A. Kutvonen, K. Fujii, and T. Sagawa, *Scientific reports* **10**, 14687 (2020).
- [62] L. Domingo, F. Borondo, G. Scialchi, A. J. Roncaglia, G. G. Carlo, and D. A. Wisniacki, *arXiv preprint arXiv:2310.00790* (2023).
- [63] K. Kobayashi and Y. Motome, *arXiv preprint arXiv:2308.00898* (2023).
- [64] S. Alipour, A. T. Rezakhani, A. P. Babu, K. Mølmer, M. Möttönen, and T. Ala-Nissila, *Phys. Rev. X* **10**, 041024 (2020).
- [65] A. P. Babu, S. Alipour, A. T. Rezakhani, and T. Ala-Nissila, *Phys. Rev. Res.* **6**, 013243 (2024).
- [66] L. Amico, R. Fazio, A. Osterloh, and V. Vedral, *Rev. Mod. Phys.* **80**, 517 (2008).
- [67] A. Peres, *Phys. Rev. Lett.* **77**, 1413 (1996).
- [68] G. Vidal and R. F. Werner, *Phys. Rev. A* **65**, 032314 (2002).
- [69] M. B. Plenio, *Phys. Rev. Lett.* **95**, 090503 (2005).
- [70] K. Audenaert, M. B. Plenio, and J. Eisert, *Phys. Rev. Lett.* **90**, 027901 (2003).
- [71] D. A. Abanin, E. Altman, I. Bloch, and M. Serbyn, *Rev. Mod. Phys.* **91**, 021001 (2019).
- [72] K. Nakajima, K. Fujii, M. Negoro, K. Mitarai, and M. Kitagawa, *Phys. Rev. Appl.* **11**, 034021 (2019).
- [73] A. Elben, S. T. Flammia, H.-Y. Huang, R. Kueng, J. Preskill, B. Vermersch, and P. Zoller, *Nature Reviews Physics* **5**, 9 (2023).
- [74] A. Elben, R. Kueng, H.-Y. R. Huang, R. van Bijnen, C. Kokail, M. Dalmonte, P. Calabrese, B. Kraus, J. Preskill, P. Zoller, and B. Vermersch, *Phys. Rev. Lett.* **125**, 200501 (2020).
- [75] Y. Li, S. Ghosh, J. Shang, Q. Xiong, and X. Zhang, *Phys. Rev. Res.* **6**, 013211 (2024).
- [76] L. Domingo, M. Grande, G. Carlo, F. Borondo, and J. Borondo, *arXiv preprint arXiv:2401.03347* (2023).
- [77] K. Kobayashi and Y. Motome, *arXiv preprint arXiv:2402.07097* (2024).
- [78] Y. Bahri, R. Vosk, E. Altman, and A. Vishwanath, *Nature Communications* **6**, 7341 (2015).

## Appendix A: Details of calculations

Here, we provide some details of our numerical calculations. As usual [5], a number of initial steps are discarded to eliminate transient effects. Specifically, we discard  $N_{\text{transient}} = 600 - 800$  steps. We use  $N_{\text{train}} = 1000 - 2000$  steps for training, where each “training steps” refers to a point in time where measurements are used to update the model’s parameters by comparing the predicted outputs to the target values. Finally,  $N_{\text{test}} = 100 - 200$  steps are reserved for testing the performance of the trained model. The training data is stored in a matrix of size  $N_O \times N_{\text{train}}$ , where the entry  $(i, j)$  represents the  $i$ -th observable measured at the  $j$ -th training step. Here,  $N_O = N_{S'} \times (N_{S'} + 1)/2$ , with  $N_O$  being the total number of measured observables and  $N_{S'}$  the number of spins in the reservoir. The reported results are averaged over 50 – 200 independent realizations of random Hamiltonians and graphs, and the averages are taken over the results of the evaluation stage. We only consider connected graphs, i.e., graphs without isolated subgraphs.

To emulate encoding errors and avoid overfitting in the training process regarding the memory task studied in the main manuscript, we add small initial noise to inputs by setting  $\eta'(t) \rightarrow \eta'(t) \pm \delta^\eta$  with  $\delta^\eta \in [0, 0.02]$ , and rescale properly. For the supervised learning, we utilize the ridge linear regression with appropriate regularization strength. For the classification of the logical multi-tasking, we use support vector machines with a nonlinear kernel [2]. In this case, the accuracy is calculated by simply matching the binary predictions with the inputs.

## Appendix B: Additional results

In this section we present supplementary data for the previously unexplored regions of the learning diagrams related to the memory task. Figure 7 shows the memory capacity for  $(\Delta^x, J^x) = (0, 0)$ , i.e., in the absence of disorder and interactions. Surprisingly, the performance declines as the graph degree increases. While we cannot provide a definitive explanation for this behavior, it may be attributed to several factors, including the specific form of the initial state, the locality of measurements, finite-size effects, and most notably, the possibility that the system is in a (dynamical) critical state in this limit. We note that this behavior is not related to integrability, as the model cannot be mapped to a free-fermionic system due to random or all-to-all connectivities. This can be further supported by calculating the gap ratio  $r_n = \min[\delta_n, \delta_{n+1}]/\max[\delta_n, \delta_{n+1}]$ , where  $n$  labels the sorted eigenvalues and  $\delta_n = E_{n+1} - E_n$ . The mean

level spacing averaged over different disordered Hamiltonians and graph realizations  $\langle r \rangle$  is  $\approx 0.39$  and  $\approx 0.53$ , for localized and ergodic phases, respectively [41]. As shown in Fig. 7(b), as disorder increases,  $\langle r \rangle$  decreases from its expected thermal value. Notably, for  $(\Delta^x, J^x) = (0, 0)$ , the gap ratio remains close to its ergodic value for all degrees. Additionally, introducing interactions deep within the localized regimes pushes the gap ratio higher, moving it closer to its ergodic value. However, a thorough investigation of this behavior would require finite-size scaling, which is beyond the scope of the current study.

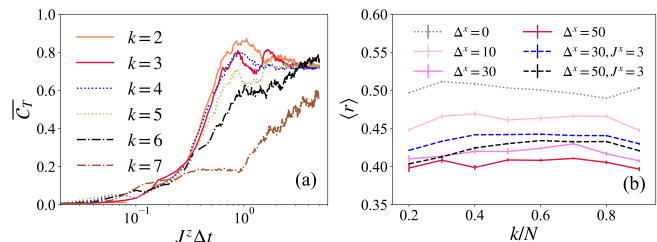


FIG. 7. (a) Normalized total memory capacity for  $N = 8$  and  $(\Delta^x, J^x) = (0, 0)$ . (b) Mean level spacing ratio for  $N = 10$ , averaged over 100 independent realizations.

Furthermore, we calculate the logarithmic negativity for the extreme cases with  $k = 2$  and  $k = N - 1$ . For  $k = 2$  and  $\Delta^x \neq 0$ , one observes a lower amount of entanglement generation between auxiliary system and the reservoir compared to the the case  $k = 3$  studied in the main text, as one might have expected. With  $k = 7$  and at finite disorder, the dynamical quantum correlations grow faster and reach higher values at finite times, compared to the former case. However, in the absence of disorder and interactions, the negativity exhibits an anomalous dynamical behavior. We have also verified that the qualitative behavior is not sensitive to the strength of the symmetry breaking term  $\Delta^z$ , which breaks the Ising  $\mathbb{Z}_2$  symmetry  $\prod_i \sigma_i^x$ . The long-time saturation value of  $\mathcal{E}_{S,S'}(t)$  is controlled solely by the system size, and thus the memory for rather long  $\mathcal{S} - \mathcal{S}'$  interaction time-scale  $\propto J^z \Delta t$  is expected to be comparable in all cases, provided that the system is not strictly localized. One should note that while having a strong entanglement is necessary for optimal learning [59], it does not guarantee it. This is reflected in the small  $\Delta^x$  region of the learning diagrams of the main text. While not crucial to the results presented in the main manuscript, the observed behavior within this parameter regime and in the limit of fully connected graphs is believed to be mostly of dynamical nature, warranting further studies. In this context, it would be insightful to investigate whether some of the observed anomalies can be accounted for by the findings presented in Ref. [39].

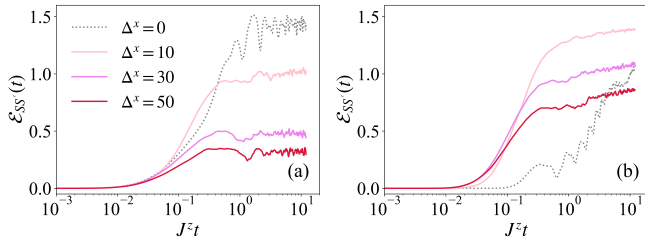


FIG. 8. (a)  $k = 2$ . (b)  $k = 7$ . For  $J^x = 0$  and  $N = 8$ .